Understanding and control of the metallic state in epitaxial NdNiO3

Guo, Qikai

DOI:
10.33612/diss.180302851

Chapter 5

From hidden metal-insulator transition to Planckian dissipation by tuning disorder

We show that heavily oxygen deficient $NdNiO_3$ (NNO) films, which are insulating due to electron localization, contain pristine regions that undergo a hidden metal-insulator transition. Increasing oxygen content increases the connectivity of the metallic regions and the metal-insulator transition is first revealed, upon reaching the percolation threshold, by the presence of hysteresis. Only upon further oxygenation is the global metallic state (with a change in the resistivity slope) eventually achieved. It is shown that sufficient oxygenation leads to linear temperature dependence of resistivity in the metallic state, with a scattering rate directly proportional to temperature. Despite the known difficulties to establish the proportionality constant, the experiments are consistent with a relationship $1/\tau = \alpha k_B T/\hbar$, with α not far from unity. These results could provide experimental support for recent theoretical predictions of disorder in a two-fluid model as a possible origin of Planckian dissipation.

5.1 Introduction

Deviations from the ideal stoichiometry in the form of oxygen vacancies (V_o), are commonly observed in perovskite oxides and, in particular, in epitaxial thin films. [1–8]. As lattice defects and source of disorder, V_o have been ever considered as detrimental to the material properties. However, later on, it is recognized that V_o can trigger interesting physical phenomena [9–16]. Among them, conducting filaments formed by V_o can stimulate an insulator-to-metal transition in metal-oxide-metal junctions [12–14]. Likewise, the intriguing resistance switching reported in field-effect transistors and junctions with oxides as the insulating layers, is also associated with the migration of V_o under electric fields [15–19]. Hence, the capability to control V_o in perovskite oxides is of importance also to explore their potentially novel functionality.

Among the perovskites, the rare-earth nickelates ($RENiO_3$) are interesting because of their tunable metal-insulator transition (MIT) [17, 20–26]. Recent seminal

works directly imaging the evolution of metal and insulating regions, have greatly contributed to a better understanding of the phase transition in these materials [27–31] but important questions remain, such as why are the metallic regions still present at low temperatures [27] or what is the origin of the critical behaviour observed at the (first-order) phase transition [30]. $RENiO_3$ are also attracting renewed attention due to the discovery of a superconducting phase in the family of the infinite-layer nickelates [32, 33], which are an oxygen deficient version of the perovskite nickelates, obtained by removal of a full layer of oxygen atoms. However, most often, V_o in nickelates are randomly distributed through the lattice, with a different effect on the transport properties [34–38]. In particular, these randomly distributed V_o are known to give rise to electron localization in defect states [34, 35, 37, 39]

In addition, NNO films have been reported to show bad metal behaviour [40], characterized by exceedingly short electron relaxation times; while in other strongly correlated materials, such as cuprate superconductors or heavy fermions, strange metal behaviour and Planckian dissipation is observed [41, 42]. This is a recent concept put forward to explain low temperature conductivity that is independent of the strength of the electron interactions and scales linearly with temperature [43, 44], defying expected quadratic Fermi liquid behaviour. However, in NNO, linear behaviour of the conductivity has only been rarely claimed [45, 46]. In NNO thin films, other scaling exponent ($1 \leq n < 2$) have also been reported [47–52], which are proposed to arise from spin fluctuations, due to the proximity to a quantum critical point, and to vary with strain [47, 48]. In addition, it has also been shown, in nickelates and in other electron correlated materials, that the apparent exponents experimentally obtained, strongly depend on the quenched disorder induced, for example, by the presence of V_o [53–55].

These findings emphasize the importance of controlling V_o in $RENiO_3$. In this work, we present a study on the effect of the oxygen content in a $NdNiO_3$ (NNO) film grown on a $YAlO_3$ (YAO) substrate under highly-compressive strain conditions, which allows us to decouple the effects of strain and disorder. Appropriate analysis of the evolution of the resistivity (ρ) versus temperature (T) curves with oxygen content offers a clear picture of the microscopic mechanisms at play, supporting the recent idea that Planckian metal behaviour can arise from a two-fluid scenario in a disorder Hubbard model [53, 56–58].

5.2 Experimental methods

Synthesis of oxygen deficient $NdNiO_{3-\delta}$ film. An epitaxial NNO film with thickness of 20 nm was deposited on a single-crystal $YAlO_3$ substrate by pulsed laser ablation of a single-phase target (Toshima Manufacturing Co., Ltd.). Before deposition,

the YAO substrates were thermally annealed at 1050 °C in a flow of O_2 and etched with DI water to obtain an atomically flat surface with single terminated terraces. The growth was performed at 700 °C with an oxygen pressure of 0.2 mbar. The laser fluence on the target was 2 J/cm^2. After deposition, the samples were cooled down to room temperature under high vacuum ($\leq 10^{-7}$ mbar) to produce an initial $NdNiO_{3-\delta}$ state with a large oxygen vacancy content. For comparison, NNO films with the same thickness were also grown on LAO and STO substrates using the same conditions. The thicknesses, crystal orientation and phase purity of the films were assessed using X-ray diffraction by means of 2θ -ω scans on a Panalytical, Xpert MRD Pro diffractometer.

Control of V_O content in film. The oxygen content in the $NdNiO_{3-\delta}$ film was tuned by annealing in an oxygen-enriched environment (400 cc/min and atmospheric pressure) with a step-by-step increased temperature. In this annealing process, the V_o in the lattice were gradually refilled with the oxygen atoms from the atmosphere (see a sketch in Fig. 5.1(a)). The content of V_o in the lattice can then decreased gradually by increasing the annealing temperature or annealing time.

Electrical properties measurement. The electrical transport properties of the film at each stage of annealing were measured between 5 K and 400 K by the van der Pauw method in a Quantum Design Physical Property Measurement System (PPMS), using a Keithley 237 current source and a Agilent 3458A multimeter. For Hall measurement, the films were patterned into Hall bar (channel dimensions 620 $\times$ 100 μm^2) using photolithography and ion etching. The Pt electrodes with a thickness of 80 nm were fabricated using e-beam evaporation to provide an ohmic contact with the film.

5.3 Results

5.3.1 Hidden metal-insulator transition.

Epitaxial $NdNiO_3$ (NNO) films are grown on $YAlO_3$ (YAO) substrates by pulsed laser deposition. A 20 nm thick NNO film is subjected to high vacuum conditions right after growth, in order to produce a large amount of V_{o} (see a sketch in Fig. 5.1). Figure 5.2(a) shows the atomic force microscopy (AFM) image of the film topography and the X-ray diffraction patterns, attesting the atomically flat, single-crystalline, epitaxial, (001)-oriented nature of the film. Then, the oxygen content is gradually increased by subjecting the same film to increasingly higher annealing temperatures (T_{a}) in an oxygen atmosphere (atmospheric pressure). As shown in Fig. 5.2(b), the (002)-diffraction peak shows a shift towards increasing angles, corresponding to a reduction in the out-of-plane lattice parameter and manifesting the decrease of V_o

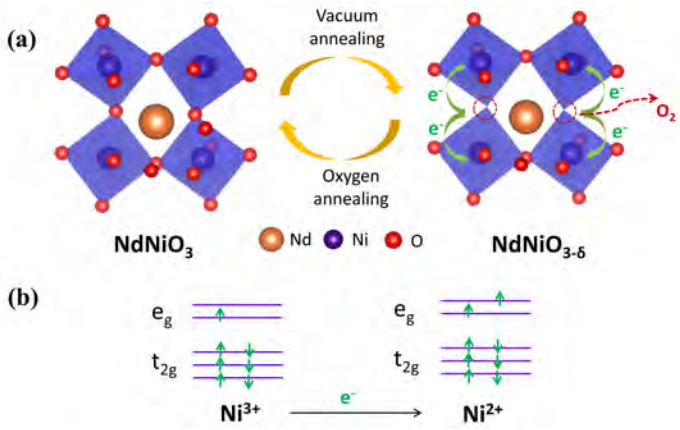

Figure 5.1: *(a) Schematic of the creation and destruction of V_o in the NNO film by the annealing process. The formation of a single oxygen vacancy donates 2 electrons to the surrounding Ni ions, decreasing their valence. (b) Occupation of Ni 3d orbitals in the Ni^{3+} state and the Ni^{2+} state.*

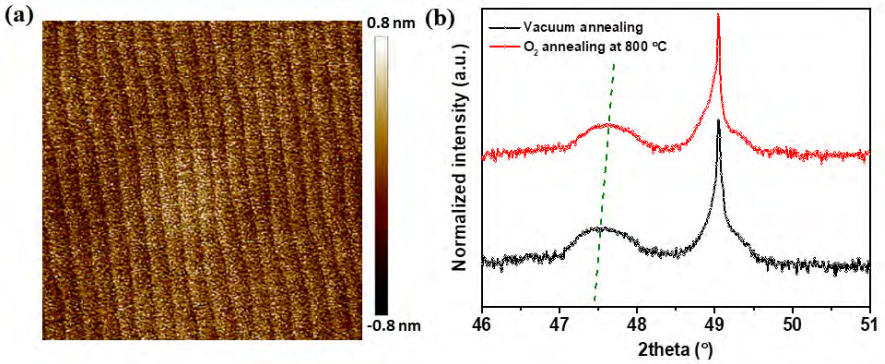

Figure 5.2: *(a) AFM topography image of a 3 × 3 μm^2 area in a 20 nm thick $NdNiO_{3-\delta}$ film grown on $YAlO_3$ substrate. (b) X-ray diffraction 2θ-ω scans around the (002) peak of a 20 nm $NdNiO_{3-\delta}$/YAO film at different annealing stages. The green dashed line shows the shift of the film peak, indicating an extended out of plane lattice in the film after vacuum annealing due to the larger concentration of oxygen vacancies.*

content in the film [34, 35].

Figure 5.3(a) shows the ρ-T curves of the NNO/YAO film measured after different annealing stages, giving rise to various oxygen content levels. The ρ-T dependence of the film annealed either in vacuum or in oxygen at a low T_a, show semiconducting behaviour, as expected for a large amount of defects [37]. In order

to observe a clear change in the sign of the resistivity derivative, a T_a of 800 °C in an oxygen-enriched environment is needed. Under these conditions the film shows a clear metal-to-insulator transition temperature (T_{MI}) at 170 K (see Fig. 5.3(d)). For intermediate states, a progressive decrease of ρ is observed under increasingly T_a, in agreement with a systematic reduction in the amount of V_o in the film. However, the temperature dependence of ρ remains insulator-like for T_a up to 700 °C.

In spite of the absence of a change in the temperature derivative of the resistivity, the existence of thermal hysteresis below 170 K, as shown in Fig. 5.3(c), for T_a above 250 °C, is consistent with the coexistence of metallic and insulating regions in an extended temperature range down to 20 K and it is a clear manifestation of the existence of the metal-insulator transition, as expected in pristine NNO [28]. In the following, we describe how the metallic regions contribute to the resistivity.

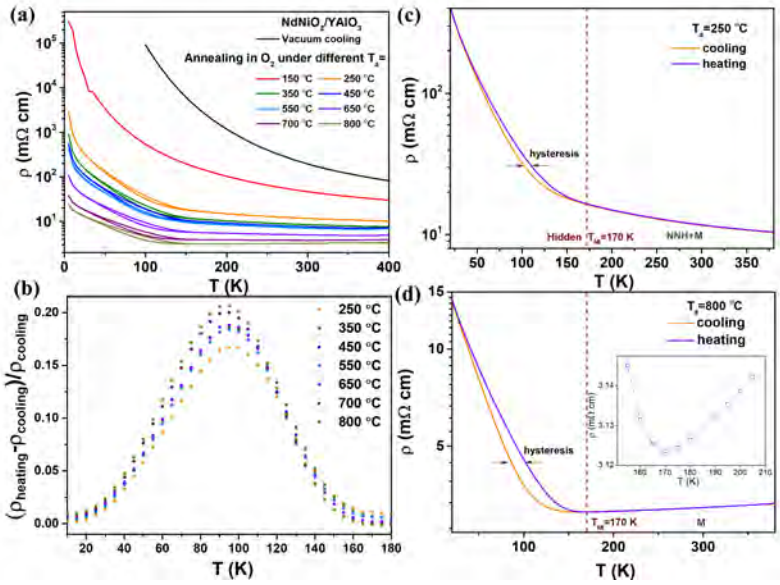

Figure 5.3: *(a) Temperature (T) dependence of resistivity (ρ) during cooling and heating for the same 20 nm thick NNO thin film grown on an YAO substrate, after annealing at increasingly larger temperatures. (b) Difference between the heating and cooling curves for all the curves in (a), emphasizing the extent of the thermal hysteresis and its independence of T_a. ρ-T measurements during heating and cooling, after annealing at (c) T_a= 250 °C and (d) T_a= 800 °C. Distinct from the film after 800 °C annealing, which shows a clear MIT, the film after 250 °C annealing shows a anomalous hysteresis when the overall MIT is still absence.*

5.3.2 Change of conduction mechanism by modulating disorder.

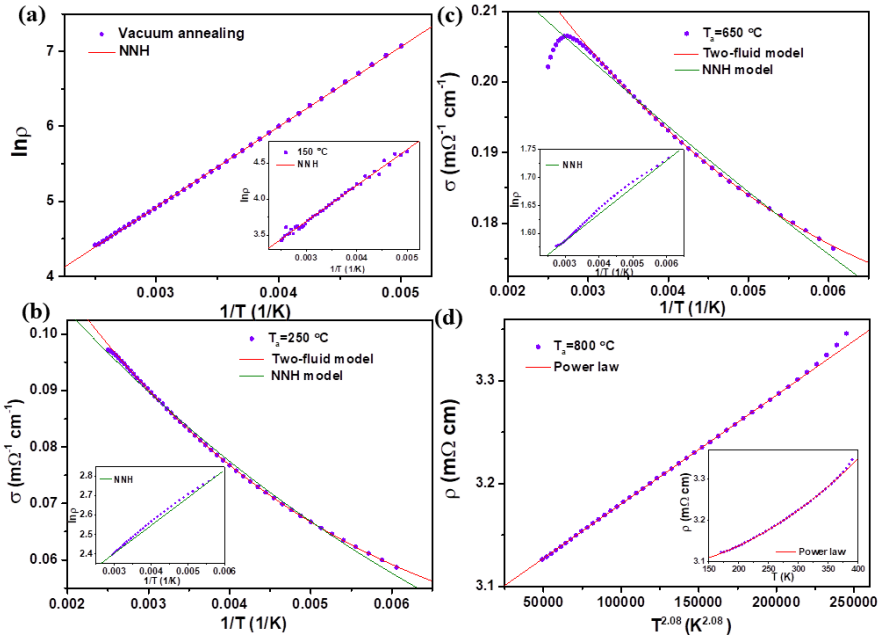

Figure 5.4: *(a) Ln(ρ)-1/T measured in the NNO/YAO film annealed in vacuum, together with the fit to a NNH model for $T \geq 170$ K. The inset shows a comparable plot for the film after T_a= 250 °C annealing. After annealing at T_a= 250 °C (b) and 650 °C (c), the conductivity (σ) versus T fits best to the two-fluid model of Eq. (5.2)). The insets in (b) and (c) plotting ln ρ versus $1/T$, highlight the inadequacy of a NNH fitting model. (d) The same NNO/YAO film after annealing at 800 °C for 1h displays a metal-like resistivity-temperature dependence (inset) with a scaling exponent n=2.08.*

As shown in Fig. 5.4(a) and Supplementary Fig. 5.1(a)-(b), the ρ-T curves of the sample cooled down from the growth in vacuum, as well as after annealing in O_2 at 150 °C (with the largest and second largest amount of V_o), follow a Nearest Neighbours Hopping (NNH) model for $T \geq 170$ K. The NNH conduction model is commonly employed in semiconducting systems [59, 60] and is described by a simple activation process:

$$\rho(T) = \rho_0 \exp(E_a/k_B T) \tag{5.1}$$

where the ρ_0 is a prefactor, E_a is the thermal activation energy of hopping electrons, and k_B is the Boltzmann constant. This model, however, does not apply to the same sample with higher oxygen contents (250 °C $\leq T_a \leq$ 650 °C), as seen from the wors-

ening of the NNH fit in Fig. 5.4(b)-(c) and Supplementary Fig. 5.1(c)-(d). Under these conditions, the film shows hysteresis in the ρ-T curve, as a clear indication of the metal-insulator transition and, thus, of the presence of metallic patches in the samples. The metallic regions are expected to change the resistivity behaviour, which deviates from the NNH model. Indeed, the data are shown to follow a two-fluid NNH+M model [53, 58, 61] that describes the combined contribution of semiconducting regions, with localized electrons (NNH) and metallic regions, with itinerant electrons (M). The total ρ is then trivially calculated by the parallel combination of these two components as:

$$\frac{1}{\rho(T)} = \frac{1}{\rho_0{}^* \exp(E_\mathrm{a}/k_\mathrm{B}T)} + \frac{1}{\rho^*(0) + A^*T^\mathrm{n}} \tag{5.2}$$

where ρ_0^* is the prefactor of the NNH contribution, normalized by geometrical factors describing the regions of defective insulating phase, while A^* measures the electron interactions in the metallic regions, normalized by a geometrical factors associated to the pristine metallic phase and $\rho^*(0)$ is the residual resistivity. For convenience, conductivity (σ) rather than ρ was used in the fitting (see Fig. 5.4(b)-(c) and Supplementary Fig. 5.1). This parallel arrangement implies that the O-Ni-O bonds in the metallic patches form a connected network in the volume between the electrodes and forming a metallic path through the sample (reaching the percolation threshold).

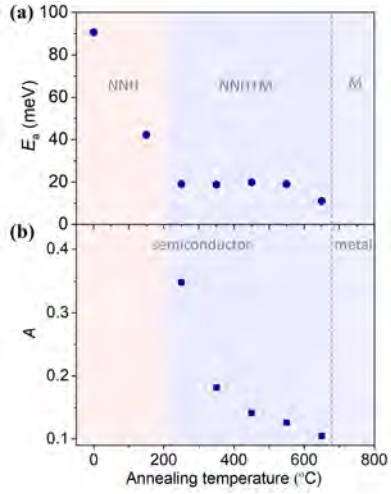

Figure 5.5: *Annealing temperature dependence of (a) the thermal activation energy E_a and (b) the A^*-coefficient for oxygen deficient NNO/YAO film extracted from the fit to the two-fluid model of Eq. 2. The A^* of 800 °C is extracted from the $\rho(T)$ of NNO/YAO film after annealing in oxygen atmosphere for 8 hours, which displays a robust linear ρ-T dependence.*

It can also be observed (see Fig. 5.3(b)) that both the local T_{MI} and the thermal hysteresis (ΔT)= 170 K - 20 K remain unchanged during oxygenation, thus, displaying no size dependence as the metallic percolated regions grow in size through the material. This shows that the material of the initial percolating metallic path has the same composition (oxygen content) as the subsequently formed paths, strongly indicating that the metallic regions are made of pristine $NdNiO_3$. Altogether, the data shows that metallic conduction at $T \geq T_{MI}$ takes place as the stoichiometric regions percolate through the sample, even if the material does not show metallic-like overall behaviour due to the presence of a too large number of V_o. The E_a and A values extracted from the fits are plotted as a function of T_a in Fig. 5.5. We will discuss these values in the *Discussion* section.

After annealing at 800 °C in a oxygen-rich atmosphere, a robust metallic behaviour of ρ is obtained in the formerly oxygen-deficient NNO film (see Fig. 5.3(d)). However, the films is not fully oxygenated yet; the V_o content can decrease further by increasing the annealing time, which is demonstrated by the progressive decrease of resistivity shown in Fig. 5.6(a). As usual, ρ- T in the metallic NNO state can be well fit with a power law added to the residual resistivity (ρ - $\rho(0) \propto AT^n$). The evolution of the extracted values of n (see Supplementary Fig. 5.2 for the method of extraction) is plotted in Fig. 5.6(b) and shows a gradual decrease with decreasing disorder, reaching n = 1 for sufficiently low vacancy content.

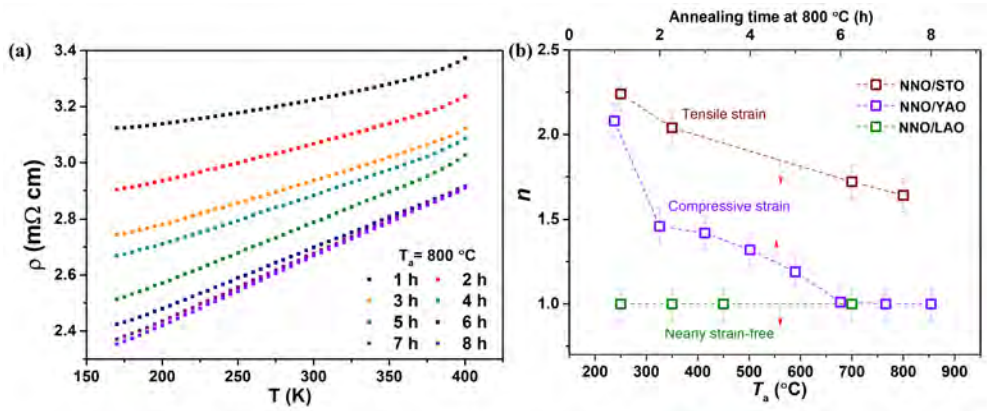

Figure 5.6: *(a) Resistivity of NNO/YAO film as a function of temperature after annealing in an oxygen-enriched environment at 800 °C with various annealing times. (b) Evolution of exponents n with the annealing process in 20 nm NNO films grown on three different substrates.*

5.3.3 Direct observation of the conduction inhomogeneity

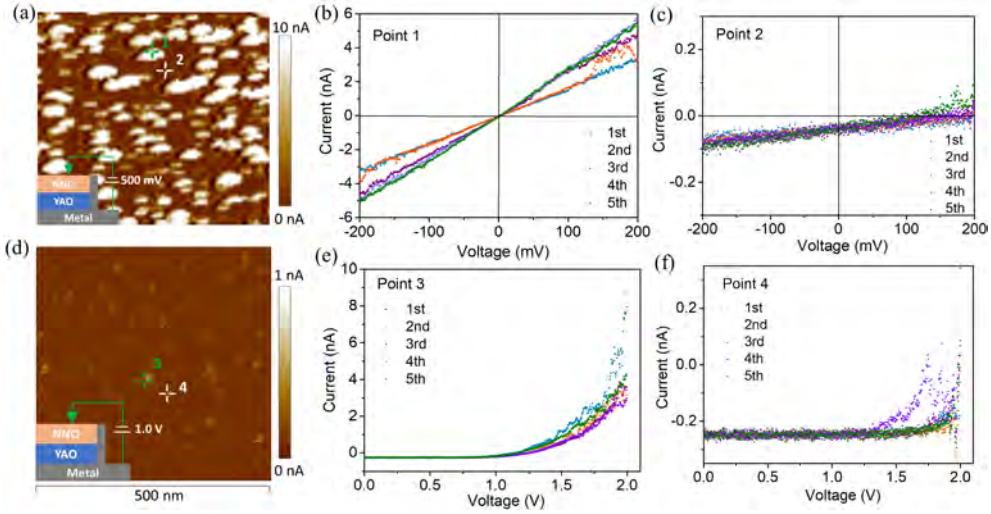

Figure 5.7: ***Conductive Atomic force microscopy (c-AFM).*** ***a*** *c-AFM image of the NNO/YAO film after annealing at 800 ° for 1 hour with a DC sample bias of 500 mV. The inset sketch illustrates the configuration of the c-AFM measurement.* ***b*** *and* ***c*** *show the I-V curves obtained from representative points 1 and 2 in* ***a****, respectively.* ***d*** *c-AFM image of the NNO/YAO film after vacuum annealing with a DC sample bias of 1.0 V.* ***e*** *and* ***f*** *show the I-V curves obtained from representative point 3 and 4 in* ***d****, respectively.*

A direct observation of the conduction inhomogeneity in oxygen-deficient NNO/YAO films was obtained by using conductive atomic force microscopy (c-AFM). During the scanning, a direct-current sample bias was applied between the tip and the sample (see a sketch in the inset of Fig. 5.7(a) and a detailed explanation in the Methods). The sample after annealing at 800 °C for 1 hour, displays two distinctly different types of regions, as shown in Fig. 5.7(a). Comparison between Fig.5.7(a) and the height map of the same area (see Supplementary Fig. 5.4) reveals that the observed contrast is not due to topographic features. *I-V* measurements were performed in two representative points (1 and 2) of Fig. 5.7(a). Notably, the current of point 1 shows a clear linear dependence with the applied voltage, indicating a robust metallic behaviour in this local area (Fig. 5.7(b)). On the contrary, the current of point 2 only displays a non-linear voltage dependence and with much smaller current values than those of point 1, reflecting semiconducting local behaviour (Fig. 5.7(c)).

A comparable measurement was also performed in the heavily oxygen-deficient NNO/YAO sample (after vacuum annealing). As shown in Fig. 5.7(d), the heavily oxygen-deficient NNO/YAO sample also presents inhomogeneous conduction.

However, even for an applied voltage of 1.0 V, significantly larger than that applied to the 800 °C annealed sample (500 mV), it shows a less conducting behaviour due to the high oxygen-deficiency. A more pronounced difference of these two states was revealed by the I-V measurements. While the current of the NNO/YAO sample after annealing at 800 °C shows a robust linear-dependence with voltage, the NNO/YAO sample after vacuum annealing displays a clear semiconductor-like performance (see Fig. 5.7(e) and 5.7(f), manifesting a distinct conduction mechanism in these two states. All of these results are well consistent with our two-fluid model discussed above.

5.3.4 Disorder tuning in various systems.

It is worthwhile to note the NNO/YAO film studied above is subjected to a ultra-large in-plane compressive strain (ε_{xx} = -3.86 %). In Chapter 4, we have revealed that the strain in epitaxial films also takes a crucial role in determining their electrical properties. Therefore, it is interesting to wonder if the oxygen vacancy also has a comparable effect on NNO films under tensile strain or on nearly strain-free systems. For this, NNO films with comparable thickness were also grown on STO (ε_{xx} = +2.7 %) and LAO (ε_{xx} = -0.3 %) substrates, respectively, and their concentration of V_o was tuned by the same method used in NNO/YAO film. The corresponding changes in structure and resistivity were characterized and shown in Fig. 5.8. As we mentioned above, the existence of oxygen vacancies gives rise to an enlarged unit cell volume of the films. This is an effect of chemical expansivity due to electrons being donated to σ bands. Hence, the change in the density of oxygen vacancies is correlated with a change of the lattice parameters of the films [34]. From Fig. 5.8(a) and (c), it is clear that the (002) diffraction peak of NNO films grown on both the STO and LAO substrates shows a shift to larger angle (smaller out-of-plane lattice parameter) after annealing in oxygen gas and high temperature, corresponding to a decrease of V_o.

Similar to what we observed in the NNO/YAO films, the resistivity of NNO/LAO and NNO/STO films also shows an reduction with the decreased V_o content (see Fig. 5.8(b) and (d)). However, a global metallic state ($\mathrm{d}\rho/\mathrm{d}T > 0$) in the latter two systems can be easily recovered after annealing at 250 °C. Note that the MIT is still suppressed in NNO/YAO film after the same annealing process and is eventually recovered only at a much larger annealing temperature (800 °C).

A more significant difference between these three systems is found in their recovered metallic phase. The extracted values of n in both the NNO/LAO and NNO/STO systems are also plotted in Fig. 5.6(b). It is clear that the n= 1 value obtained in a nearly strain-free system (NNO/LAO) is unchanged with the further annealing. On the contrary, a clear change of n is achieved with the films under large tensile strain (NNO/STO), or for the compressively strained films (NNO/YAO). The NNO/STO

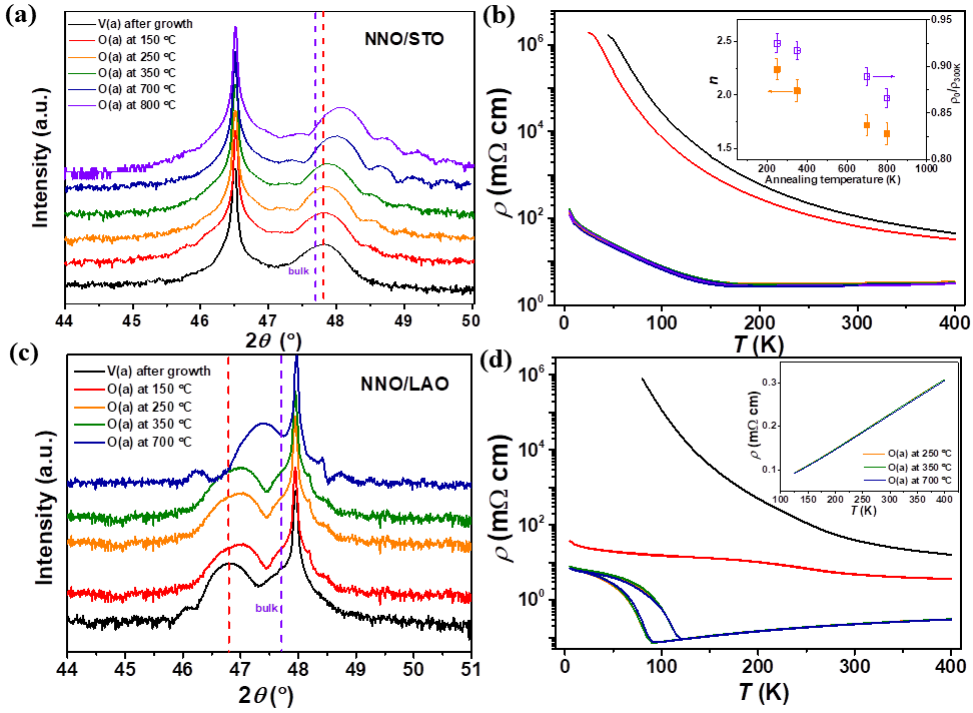

Figure 5.8: *Structural and electrical characterization of oxygen-deficient nickelate films. XRD $2\theta - \omega$ scans around the (002) peaks of a 20 nm NNO/STO (a) and NNO/LAO (b) film at various annealing stages. The red dashed lines indicate the position of the (002) peak of NNO films after vacuum annealing (V(a)), while the purple dashed lines point out the peak position of bulk NNO. After annealing in an oxygen-enriched environment (O(a)), at increasingly larger temperatrues, the (002) peak shows a clear shift to larger angles. The resistivity as a function of temperature of the NNO/STO and NNO/LAO films for the various annealing temperatures are shown in (c) and (d), respectively. The inset of (c) shows the extracted exponents (left axis) and residual resistivity ratio (right axis) in the metallic phase of the NNO/STO film, as a function of annealing temperature. The error bar was determined from the fit to experimental data. The inset of (d) reveals the linear-T dependence of resistivity in the metallic phase of the NNO/LAO film after annealing.*

films used here (with similar thickness as the other two types) do not reach the n= 1 value due to the fact that oxygen vacancies are utilize to achieve epitaxial lattice matching and refilling them is not possible while maintaining the structural integrity. However, it was shown that thicker (less strained) films on STO do achieve the n= 1 exponent [55].

5.4 Discussion

5.4.1 Double percolation model.

Our results are consistent with a description of oxygenation as a percolative process (see a sketch in Fig. 5.9). In the initial state, the NNO film after vacuum cooling possesses a large amount of Ni^{2+}, acting as a semiconducting matrix (grey regions in Fig. 5.9). The ρ-T then follows a NNH model for T >170 K (which is the T_{MI} of the nearly-stoichiometric film), while a Variable Range Hopping (VRH) mechanism is found to dominate in the lower temperature range (see Supplementary Fig. 5.3), indicating a change in hopping behaviour as a precursor of the metal-insulator transition, even if no metallic behaviour is yet observed. For T_a= 250 °C, the first percolation paths of stoichiometric regions form across the film. Above T_{MI}, these paths are metallic but, as they are surrounded by the dominant insulating (defective) matrix, the film still shows semiconductor character ($\mathrm{d}\rho(T)/\mathrm{d}T < 0$). Indeed, an excellent fit to the data is presented by an NNH+M two-fluid model, which includes itinerant electron metallic resistance in parallel with the resistance contributed by regions that host localized hopping electrons, for all intermediate T_a= 250 °C - 650 °C. For each stage of annealing, and upon decreasing the environment temperature, the stoichiometric percolation paths undergo a metal-insulator transition, which is visible as a thermal hysteresis below the local T_{MI} (marked by green solid lines in Fig. 5.9). For sufficiently long annealing at 800 °C, the metallic regions cover large enough volume ratio to show a sign change in the ρ-T slope (($\mathrm{d}\rho(T)/\mathrm{d}T > 0$)). This is in agreement with previous reports of NNO films grown on YAO substrates showing a robust metallic ρ-T dependence [47, 48, 62].

The progressive oxygenation of the non-stoichiometric matrix is accompanied by a local transformations of different types of polyhedra (see a schematic of four possible coordination types in Fig. 5.10). In nickelates, oxygen-deficiency leads to a square pyramidal NiO_5 coordination. NiO_4, with either tetrahedral or square-planar configurations, can be formed if two oxygen atoms of the same octahedra are removed [37]. In heavily deficient cases, the transformation from NiO_4 to NiO_5 coordination could also be expected. This change in the type of polyhedra could be the reason for the observed change in E_a with T_a in the first two states (see Fig. 5.5), different from the constant value of E_a in the intermediate annealing states. $E_a \simeq 20$ meV is consistent with those reported in the normal semiconducting phases of nickelates [63–66]. However, a clear evolution of the A^*-coefficients with decreasing V_o is observed in the intermediate states, indicating a progressive increase of the volume fraction of metallic regions, as expected.

While the metal-insulator transition is clearly of first-order, the order of the percolation transition under oxygenation still needs investigation. A second-order perco-

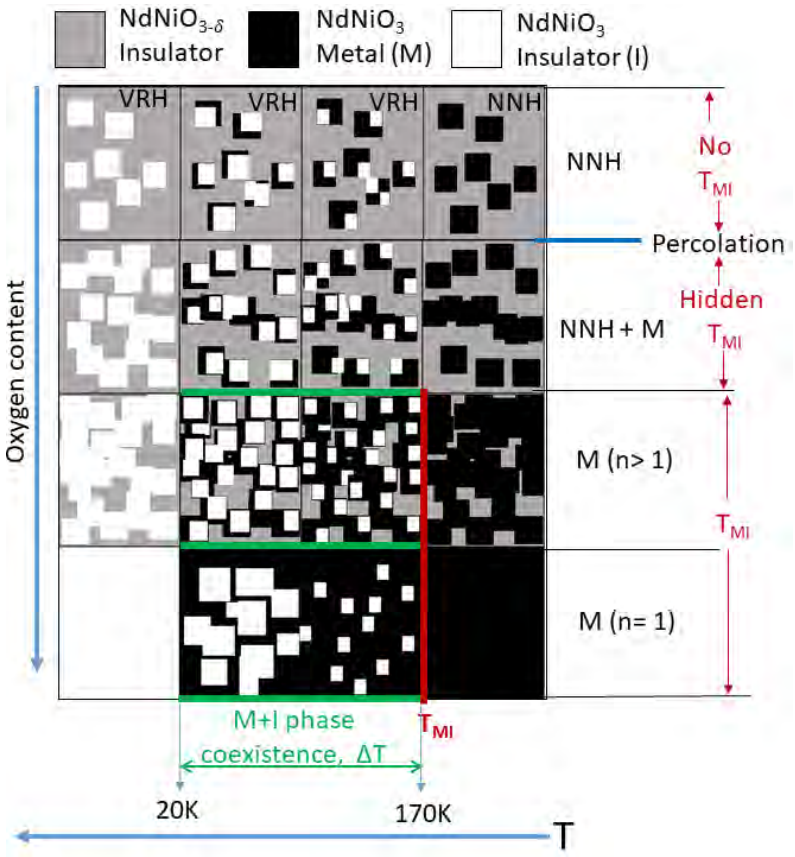

Figure 5.9: *Illustration of the evolution of NNO films as a function of oxygen content (vertical) and temperature (horizontal). Grey, black and white denote electron-localized (defective) $NdNiO_{3-\delta}$, metallic $NdNiO_3$ and insulating $NdNiO_3$, respectively. For $T \geq 170$ K, the evolution of conduction models as a function of oxygen content (from NNH to NNH+M to M) are denoted. For highly defective films the data are consistent with a semiconducting NNH and VRH process above and below 170K, respectively. When the oxygen content is sufficient to barely allow percolation of the metallic regions (blue horizontal line), the system still displays a semiconductor-like behaviour and follows a two-fluid NNH+M model. However, the MIT happens already locally through a nucleation and growth (first-order) process, visible through the hysteresis that denotes the coexistence range (green horizontal line). After enough percolation paths have formed, a measurable T_{MI} appears (red vertical lines) but the ρ scaling exponent is seen to decrease with further oxygenation, reaching n= 1 for the most stoichiometric case.*

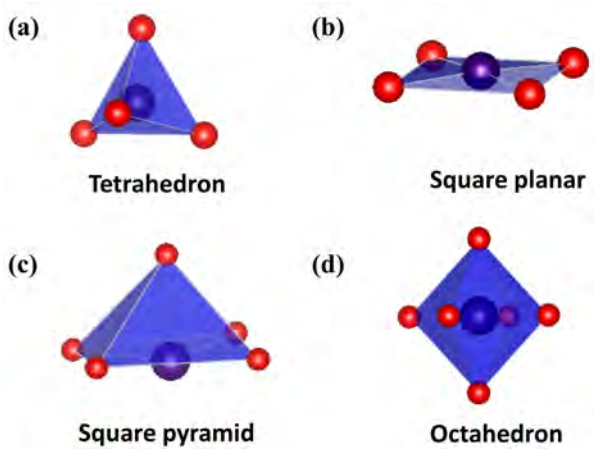

Figure 5.10: *Schematic of four possible coordination types may exist in the lattice of oxygen-deficient NNO film.*

lation transition, as in VO_2 [67], could offer an alternative explanation for the fractal antiferromagnetic structures observed in ref. [30]. This could perhaps also explain the coexistence of first-order and second-order features also reported in these materials [29].

5.4.2 Underlying physics behind the strange linear-T resistivity.

Finally, we discuss the temperature scaling of ρ in the recovered metallic state of annealed NNO films on YAO (under compressive strain) in Fig. 5.6. In the same figure, we add the NNO films on STO substrates (NNO/STO), under tensile strain, and on LAO substrates (NNO/LAO), nearly strain-free. In the latter, the scaling of $\rho(T)$ is independent of the T_a and gives rise to n=1 [55], as in the bulk material [45, 46] and in agreement with ref. [48]. We believe this is attributed to a low V_o content compared with the other two systems, which is supported by values of ρ that are one order of magnitude lower in the metallic state of NNO/LAO film compared with that of the NNO/STO and NNO/YAO films under strain. In the case of tensile strained films (NNO/STO), strain and defect formation are correlated since defects are created during growth as a mechanism to enlarge the lattice and achieve epitaxy [55]. In the current case of compressively strained NNO/YAO, there is no natural tendency for the film to favor vacancies, so these can be created and removed purposely, and the effects of strain and oxygen content can be separated, as shown in Fig. 5.6.

The validity of the n = 1 exponent from above the T_{MI}= 170 K (and even from T_{MI}= 100 K in NNO/LAO), significantly smaller than the Debye temperature of the

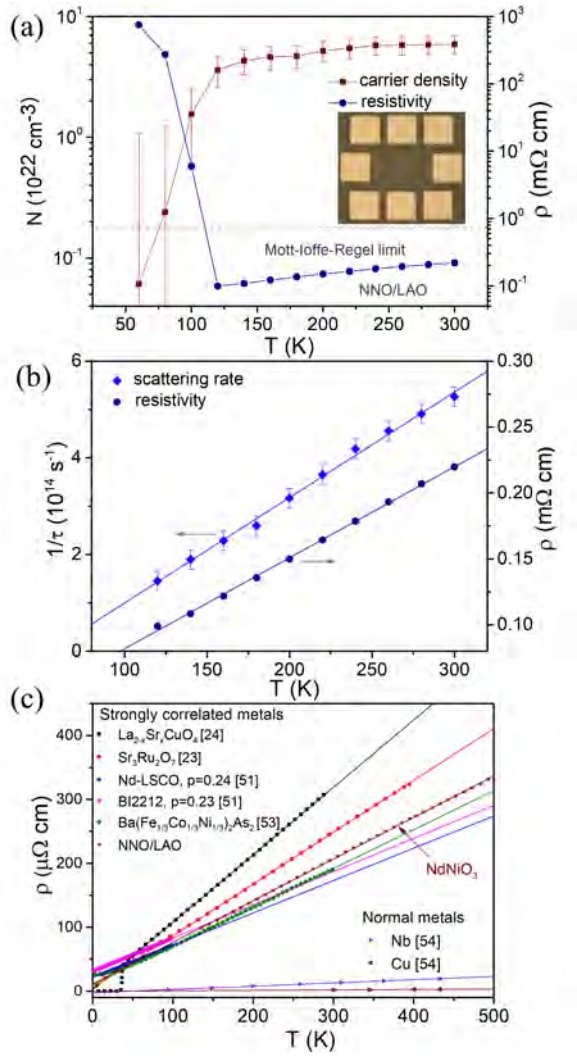

Figure 5.11: *(a) Log of carrier density and log of resistivity of a 5 nm NNO/LAO film as a function of temperature. The inset shows the Hall bar used, with channel dimensions 620 × 100 μm^2. The dashed line indicates the Mott-Ioffe-Regel limit in nickelates [40, 47]. (b) $1/\tau$ as a function of temperature is plotted together with the resistivity and their linear fits. Inset shows a fit of resistivity till to 0 K. (c) The T-linear resistivities of reported Planckian metals [41, 42, 68–70] together with that of the NNO/LAO film. (Data source: Cu, Nb, Nb_3Sb [**?**], $La_{2-x}Sr_xCuO_4$ [42], Nd-LSCO (p=0.24) and Bi2212 (p=0.23) [68], $Ba(Fe_{1/3}Co_{1/3}Ni_{1/3})_2As_2$ [69], $Sr_3Ru_2O_7$, [41].)*

material (420 K [45, 48]), casts questions about its origin being on electron-phonon interactions and points to the strange metal behaviour of $NdNiO_3$. Strange metal behaviour is characterized by Planckian dissipation, whose origin is still under debate [43], that supports a resistivity that scales linearly with temperature and is independent of the nature of the electron interactions. Recent theoretical calculations have shown that Planckian metal behaviour can also originate from a disordered Hubbard model (with electron interactions that do not conserve momentum), from which a two-fluid model emerges that consists of localized Sachdev-Ye-Kitaev (SYK) islands interacting with itinerant fermions [30, 56, 57]. Our results seem consistent with this scenario.

To explicate the underlying physics behind this strange linear-T-resistivity, we use a NNO film grown under low strain conditions on LAO substrate to reduce the defect content to the minimum. Cross-sectional HAAFAF-STEM characterizations discussed in chapter 3 and 4 indicate perfectly epitaxial growth with atomically flat interfaces and a pure phase of this film. Commonly reported lattice imperfections in nickelates, such as dislocations and Ruddlesden-Popper faults, are not observed. The low concentration of the lattice defects present is also supported by the ultra-low residual resistivity ($e.g$ 8.6 $\pm$0.22 $\mu\Omega$ cm in the 5 nm film), as shown in Supplementary Fig. S5. Moreover, the ρ values of the NNO/LAO films are well below the Mott-Ioffe-Regel limit [40, 47] and display a robust linear-T dependence (from 120 to 500 K). All these features make it an ideal candidate to study the intrinsic origin of the linear-T-resistivity in this material.

Hall measurements shown in Fig. 5.11(a) display a nearly constant value (within error bars) of the carrier density (N) in the metallic state, with the expected sharp decrease at and below T_{MI}. We note that the measured N values are larger than those expected from 1 e per Ni atom. This discrepancy could be due to the existence of both electron-like and hole-like states at the E_{F} [40] or to strong polaronic effects in the metallic state [71], which make reliable measurements of carrier density challenging in nickelates [21].

$1/\tau$ values obtained from these measurements, using Drude's formula ρ = m*/N $e^2\tau$ and the reported $m^* = 7m_o$ [40], show linear behaviour (see Fig. 5.11(b)) and nearly follows the universal dissipation law, $1/\tau = \alpha k_B T/\hbar$, with a constant α= 9.3$\pm$ 4.0, larger than that expected in Planckian metals [41, 44, 68, 72]. However, if a more physically meaningful value of the carrier density is used (N= 1.0$\times$ 10^{22}cm^{-3} [40, 71]), a values of α= 1.8$\pm$ 0.4, in the proximity of the Planckian dissipation bound (α= 1) is obtained. Indeed, the behaviour of $NdNiO_3$ is comparable to that of other reported Planckian metals, in the same temperature range, as shown in Fig. 5.11(c), as well as in Table 1 [41, 42, 68–70]. Our observations, therefore, suggest that further work is required to fully understand the metallicity of this materials family.

Table 5.1: *Relevant parameters for different reported Planckian metals and the $NdNiO_3$ films presented in this work. For the definitions of the various parameters, see main text. (Note: the error bar of N is obtained from the uncertainty of the measurement, the error bar of m^* is determined by the different values reported in different works, the error bar of A is obtained from the fit to resistivity, and the error bars of α is calculated from the uncertainty of parameters mentioned above.)*

Material	N(10^{28}m^{-3})	m*/m$_0$	A ($\mu\Omega$ cm/K)	α
Bi2212 (p=0.23)[68]	0.68	8.4	0.62	1.1
Nd-LSCO (p=0.24)[68]	0.79	12	0.49	0.7
$Sr_3Ru_2O_7$[41]	–	–	1.1	1.5
$(TMTSF)_2PF_6$[41]	0.136	–	0.38	0.9
$BaFe_2(P_{0.3}As_{0.7})_2$[41]	–	–	1.1	2.2
$CeCoIn_5$[41]	–	–	1.6	1.0
Cu[41]	8.5	1.3	0.007	1.0
Nb[41]	–	–	0.049	2.3
$NdNiO_3$	5.0 ± 1.0[this work]	7 ± 1[40, 73]	0.6 ± 0.1[this work]	9.3 ± 4.0
$NdNiO_3$	1.0 [40, 71]	7 ± 1[40, 73]	0.6 ± 0.1[this work]	1.8 ± 0.4

5.5 Conclusion

To conclude, in oxygen deficient $NdNiO_3$, metallic regions coexisting with semiconducting defective regions, undergo local metal-insulator transitions, visible above the percolation threshold as thermal hysteresis in the resistivity. Only by further increasing the volume fraction of the pristine state, the metal-insulator transition is unveiled as a change in the slope sign of the resistivity. The n= 1 ρ-T exponent is recovered upon sufficient oxygenation. This establishes the intrinsic T-linear resistivity in metallic $NdNiO_3$ and postulates its strange metal behavior. Although reliable quantification of the carrier density and the value of α in nickelates remains challenging, these results provide experimental support for the disorder-induced two-fluid origin of Planckian dissipation.

5.6 Supplementary figures

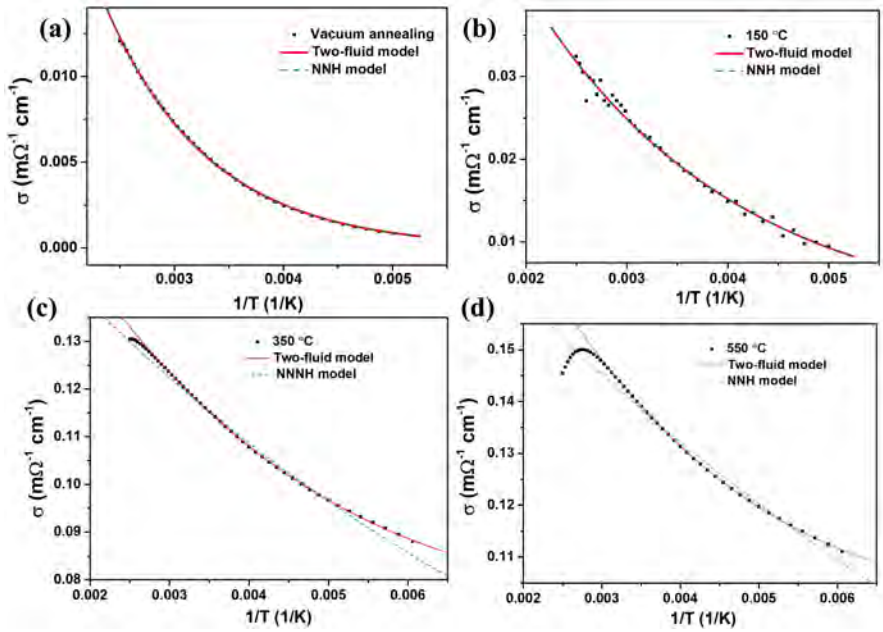

Figure 5.1: *σ versus T^{-1} plot for as-prepared $NdNiO_{3-\delta}/YAlO_3$ film after vacuum annealing (a) and O_2 annealing at (b) 150 °C, (c) 350 °C, and (d) 550 °C. The red solid lines indicate a fit to the experimental data by employing the two-fluid model in Eq.(2), while the green dashed lines are the fit to NNH model. The fits to both models coincide in (a) and (b), indicating the negligible contributions of power law (metallic regions) to the fit. On the contrary, the conductivity in (c) and (d) can only be described by the two-fluid model, emphasizing the importance of power law (metallic regions) to the fit.*

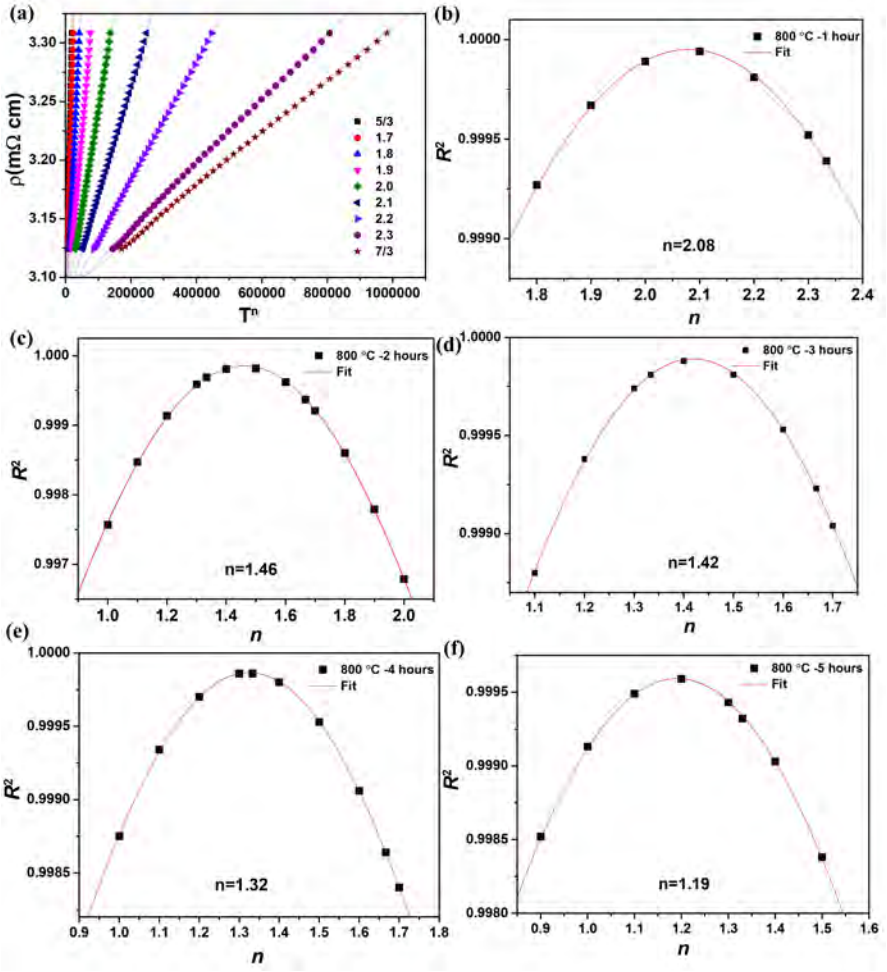

Figure 5.2: *Extraction of exponents (n). Resistivity of a 20 nm $NdNiO_{3-\delta}/YAlO_3$ film (after annealing at 800 °C for 1 hour) as a function of T^n with different n values. (b-f) The coefficient of determination (R^2) as a function of n for the same $NdNiO_{3-\delta}/YAlO_3$ film annealed at 800 °C for (b) 1 hour, (c) 2 hours, (d) 3 hours, (e) 4 hours, (f) 5 hours, respectively.*

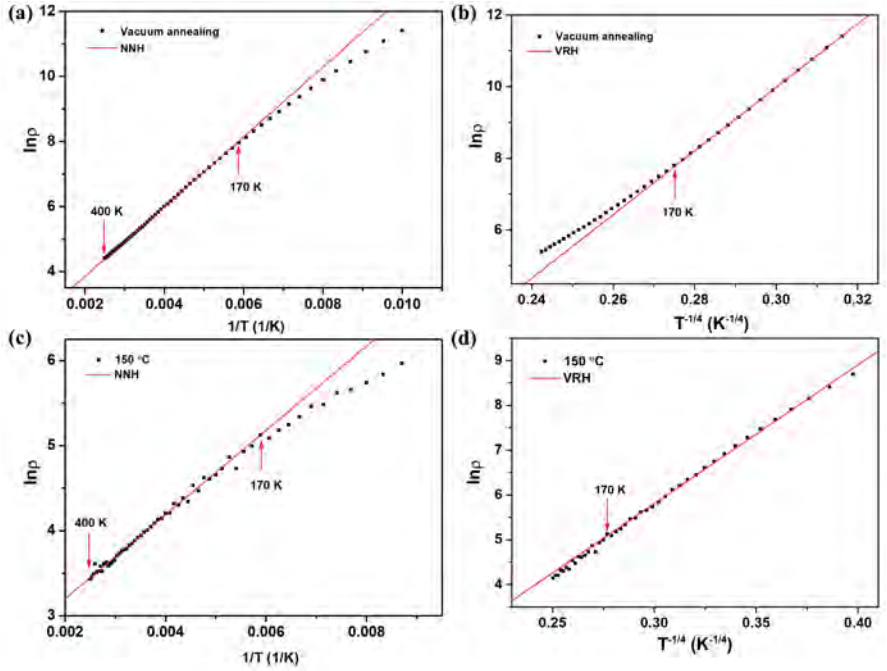

Figure 5.3: *(a) $ln\rho$ versus T^{-1} and (b) $ln\rho$ versus $T^{-1/4}$ for a NNO/YAO film after vacuum annealing. (c) $ln\rho$ versus T^{-1} and (d) $ln\rho$ versus $T^{-1/4}$ for the same NNO/YAO film after annealed in O_2 at 150 °C. The curve is well described by the Near Neighbours Hopping (NNH) model for the temperature range above 170 K, while the Variable Range Hopping (VRH) is applied in the temperature range below 170 K.*

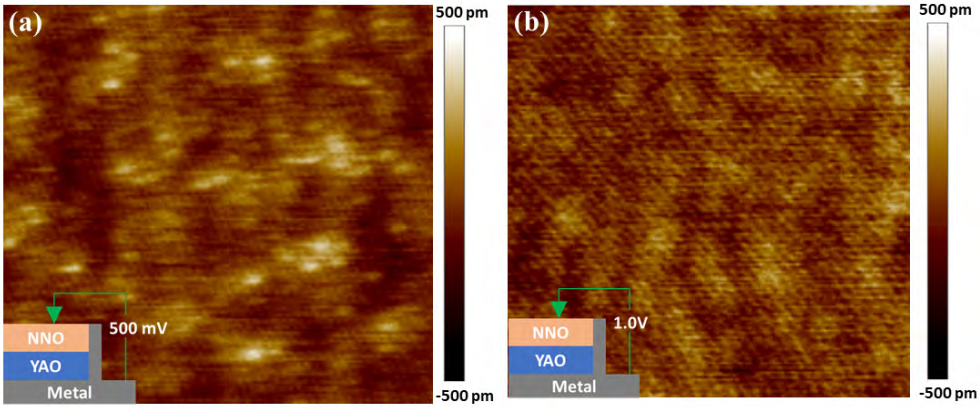

Figure 5.4: *Topography captured in the conductive atomic force microscopy (c-AFM) of the $NdNiO_3/YAlO_3$ film after annealing at 800 °C for 1 hour* ***a*** *and after vacuum annealing* ***b****. The inset sketches illustrate the configuration and the applied bias in the c-AFM measurement.*

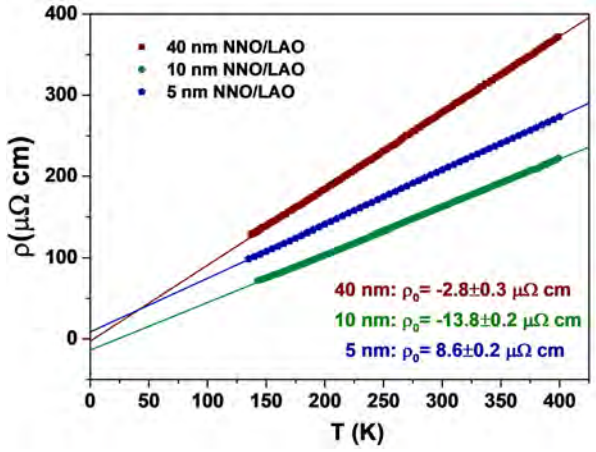

Figure 5.5: *Resistivity of $NdNiO_3$ films grown on $LaAlO_3$ substrates with different thickness. The solid lines are fit to the resistivity with a power law ($\rho=\rho_0+AT$). Notably, the values of the residual resistivity in our $NdNiO_3/LaAlO_3$ films are quite small, indicating a small content of lattice disorders. It is worth noticing that the negative values of the resistivity can be explained by the need of including the Fermi-liquid term in the fit (see Chapter 6).*

Bibliography

[1] D. A. Muller, N. Nakagawa, A. Ohtomo, J. L. Grazul, and H. Y. Hwang, "Atomic-scale imaging of nanoengineered oxygen vacancy profiles in $SrTiO_3$," *Nature* **430**(7000), pp. 657–661, 2004.

[2] W. L. Warren, K. Vanheusden, D. Dimos, G. E. Pike, and B. A. Tuttle, "Oxygen vacancy motion in perovskite oxides," *Journal of the American Ceramic Society* **79**(2), pp. 536–538, 1996.

[3] C. Park and D. Chadi, "Microscopic study of oxygen-vacancy defects in ferroelectric perovskites," *Physical Review B* **57**(22), p. R13961, 1998.

[4] J. Scott and M. Dawber, "Oxygen-vacancy ordering as a fatigue mechanism in perovskite ferroelectrics," *Applied Physics Letters* **76**(25), pp. 3801–3803, 2000.

[5] R. Klie, Y. Ito, S. Stemmer, and N. Browning, "Observation of oxygen vacancy ordering and segregation in perovskite oxides," *Ultramicroscopy* **86**(3-4), pp. 289–302, 2001.

[6] C. Cazorla, "Lattice effects on the formation of oxygen vacancies in perovskite thin films," *Physical Review Applied* **7**(4), p. 044025, 2017.

[7] H. Jeen, W. S. Choi, M. D. Biegalski, C. M. Folkman, I.-C. Tung, D. D. Fong, J. W. Freeland, D. Shin, H. Ohta, M. F. Chisholm, *et al.*, "Reversible redox reactions in an epitaxially stabilized $SrCoO_x$ oxygen sponge," *Nature materials* **12**(11), pp. 1057–1063, 2013.

[8] P. Agrawal, J. Guo, P. Yu, C. Hébert, D. Passerone, R. Erni, and M. Rossell, "Strain-driven oxygen deficiency in multiferroic $SrMnO_3$ thin films," *Physical Review B* **94**(10), p. 104101, 2016.

[9] D. Kan, T. Terashima, R. Kanda, A. Masuno, K. Tanaka, S. Chu, H. Kan, A. Ishizumi, Y. Kanemitsu, Y. Shimakawa, *et al.*, "Blue-light emission at room temperature from Ar^+-irradiated $SrTiO_3$," *Nature materials* **4**(11), pp. 816–819, 2005.

[10] J. Jeong, N. Aetukuri, T. Graf, T. D. Schladt, M. G. Samant, and S. S. Parkin, "Suppression of metal-insulator transition in VO_2 by electric field-induced oxygen vacancy formation," *Science* **339**(6126), pp. 1402–1405, 2013.

[11] A. Kalabukhov, R. Gunnarsson, J. Börjesson, E. Olsson, T. Claeson, and D. Winkler, "Effect of oxygen vacancies in the $SrTiO_3$ substrate on the electrical properties of the $LaAlO_3$/ $SrTiO_3$ interface," *Physical Review B* **75**(12), p. 121404, 2007.

[12] K. Szot, W. Speier, R. Carius, U. Zastrow, and W. Beyer, "Localized metallic conductivity and self-healing during thermal reduction of $SrTiO_3$," *Physical review letters* **88**(7), p. 075508, 2002.

[13] M. Janousch, G. I. Meijer, U. Staub, B. Delley, S. F. Karg, and B. P. Andreasson, "Role of oxygen vacancies in Cr-doped $SrTiO_3$ for resistance-change memory," *Advanced materials* **19**(17), pp. 2232–2235, 2007.

[14] K. Szot, W. Speier, G. Bihlmayer, and R. Waser, "Switching the electrical resistance of individual dislocations in single-crystalline $SrTiO_3$," *Nature materials* **5**(4), pp. 312–320, 2006.

[15] Z. Xu, K. Jin, L. Gu, Y. Jin, C. Ge, C. Wang, H. Guo, H. Lu, R. Zhao, and G. Yang, "Evidence for a crucial role played by oxygen vacancies in $LaMnO_3$ resistive switching memories," *small* **8**(8), pp. 1279–1284, 2012.

[16] J. J. Yang, M. D. Pickett, X. Li, D. A. Ohlberg, D. R. Stewart, and R. S. Williams, "Memristive switching mechanism for metal/oxide/metal nanodevices," *Nature nanotechnology* **3**(7), pp. 429–433, 2008.

[17] J. Shi, S. D. Ha, Y. Zhou, F. Schoofs, and S. Ramanathan, "A correlated nickelate synaptic transistor," *Nat. Commun.* **4**(1), pp. 1–9, 2013.

[18] V. Rouco, R. El Hage, A. Sander, J. Grandal, K. Seurre, X. Palermo, J. Briatico, S. Collin, J. Trastoy, K. Bouzehouane, *et al.*, "Quasiparticle tunnel electroresistance in superconducting junctions," *Nature communications* **11**(1), pp. 1–9, 2020.

[19] U. Bauer, L. Yao, A. J. Tan, P. Agrawal, S. Emori, H. L. Tuller, S. Van Dijken, and G. S. Beach, "Magneto-ionic control of interfacial magnetism," *Nature materials* **14**(2), pp. 174–181, 2015.

[20] P. Canfield, J. Thompson, S.-W. Cheong, and L. Rupp, "Extraordinary pressure dependence of the metal-to-insulator transition in the charge-transfer compounds $NdNiO_3$ and $PrNiO_3$," *Phys. Rev. B* **47**(18), p. 12357, 1993.

[21] S. Catalano, M. Gibert, J. Fowlie, J. Iniguez, J.-M. Triscone, and J. Kreisel, "Rare-earth nickelates $RNiO_3$: thin films and heterostructures," *Rep. Prog. Phys.* **81**(4), p. 046501, 2018.

[22] M. Amboage, M. Hanfland, J. Alonso, and M. Martinez-Lope, "High pressure structural study of $SmNiO_3$," *J. Phys. Conden. Matt.* **17**(11), p. S783, 2005.

[23] S. D. Ha, U. Vetter, J. Shi, and S. Ramanathan, "Electrostatic gating of metallic and insulating phases in $SmNiO_3$ ultrathin films," *Appl. Phys. Lett.* **102**(18), p. 183102, 2013.

[24] S. Bubel, A. J. Hauser, A. M. Glaudell, T. E. Mates, S. Stemmer, and M. L. Chabinyc, "The electrochemical impact on electrostatic modulation of the metal-insulator transition in nickelates," *Appl. Phys. Lett.* **106**(12), p. 122102, 2015.

[25] S. K. Ojha, S. Ray, T. Das, S. Middey, S. Sarkar, P. Mahadevan, Z. Wang, Y. Zhu, X. Liu, M. Kareev, *et al.*, "Anomalous electron transport in epitaxial $NdNiO_3$ films," *Phys. Rev. B* **99**(23), p. 235153, 2019.

[26] C. Domínguez, A. B. Georgescu, B. Mundet, Y. Zhang, J. Fowlie, A. Mercy, A. Waelchli, S. Catalano, D. T. Alexander, P. Ghosez, *et al.*, "Length scales of interfacial coupling between metal and insulator phases in oxides," *Nat. Mater.* , pp. 1–6, 2020.

[27] G. Mattoni, P. Zubko, F. Maccherozzi, A. J. van der Torren, D. B. Boltje, M. Hadjimichael, N. Manca, S. Catalano, M. Gibert, Y. Liu, *et al.*, "Striped nanoscale phase separation at the metal-insulator transition of heteroepitaxial nickelates," *Nat. Commun.* **7**(1), pp. 1–7, 2016.

[28] D. Preziosi, L. Lopez-Mir, X. Li, T. Cornelissen, J. H. Lee, F. Trier, K. Bouzehouane, S. Valencia, A. Gloter, A. Barthélémy, *et al.*, "Direct mapping of phase separation across the metal-insulator transition of $NdNiO_3$," *Nano Lett.* **18**(4), pp. 2226–2232, 2018.

[29] K. Post, A. McLeod, M. Hepting, M. Bluschke, Y. Wang, G. Cristiani, G. Logvenov, A. Charnukha, G. Ni, P. Radhakrishnan, *et al.*, "Coexisting first-and second-order electronic phase transitions in a correlated oxide," *Nat. Phys.* **14**(10), pp. 1056–1061, 2018.

[30] J. Li, J. Pelliciari, C. Mazzoli, S. Catalano, F. Simmons, J. T. Sadowski, A. Levitan, M. Gibert, E. Carlson, J.-M. Triscone, *et al.*, "Scale-invariant magnetic textures in the strongly correlated oxide $NdNiO_3$," *Nat. Commun.* **10**(1), pp. 1–7, 2019.

[31] J. H. Lee, F. Trier, T. Cornelissen, D. Preziosi, K. Bouzehouane, S. Fusil, S. Valencia, and M. Bibes, "Imaging and harnessing percolation at the metal-insulator transition of $NdNiO_3$ nanogaps," *Nano Lett.* **19**(11), pp. 7801–7805, 2019.

[32] D. Li, K. Lee, B. Y. Wang, M. Osada, S. Crossley, H. R. Lee, Y. Cui, Y. Hikita, and H. Y. Hwang, "Superconductivity in an infinite-layer nickelate," *Nature* **572**(7771), pp. 624–627, 2019.

[33] M. Osada, B. Y. Wang, B. H. Goodge, K. Lee, H. Yoon, K. Sakuma, D. Li, M. Miura, L. F. Kourkoutis, and H. Y. Hwang, "A superconducting praseodymium nickelate with infinite layer structure," *Nano Lett.* **20**(8), pp. 5735–5740, 2020.

[34] L. Wang, S. Dash, L. Chang, L. You, Y. Feng, X. He, K.-j. Jin, Y. Zhou, H. G. Ong, P. Ren, *et al.*, "Oxygen vacancy induced room-temperature metal–insulator transition in nickelate films and its potential application in photovoltaics," *ACS Appl. Mater. Interfaces* **8**(15), pp. 9769–9776, 2016.

[35] S. Heo, C. Oh, J. Son, and H. M. Jang, "Influence of tensile-strain-induced oxygen deficiency on metal-insulator transitions in $NdNiO_{3-\delta}$ epitaxial thin films," *Sci. Rep.* **7**(1), pp. 1–9, 2017.

[36] T. Onozuka, A. Chikamatsu, T. Katayama, Y. Hirose, I. Harayama, D. Sekiba, E. Ikenaga, M. Minohara, H. Kumigashira, and T. Hasegawa, "Reversible changes in resistance of perovskite nickelate $NdNiO_3$ thin films induced by fluorine substitution," *ACS Appl. Mater. Interfaces* **9**(12), pp. 10882–10887, 2017.

[37] M. Kotiuga, Z. Zhang, J. Li, F. Rodolakis, H. Zhou, R. Sutarto, F. He, Q. Wang, Y. Sun, Y. Wang, *et al.*, "Carrier localization in perovskite nickelates from oxygen vacancies," *Proc. Natl. Acad. Sci. USA* **116**(44), pp. 21992–21997, 2019.

[38] Y. Zhang, Y. Cao, H. Hu, X. Wang, P. Li, Y. Yang, J. Zheng, C. Zhang, Z. Song, A. Li, *et al.*, "Flexible metal-insulator transitions based on van der waals oxide heterostructures," *ACS Appl. Mater. Interfaces* **11**(8), pp. 8284–8290, 2019.

[39] S. Harisankar, K. Soni, E. Yadav, and K. R. Mavani, "Strain-mediated effects of oxygen deficiency and variation in non-Fermi liquid behavior of epitaxial $PrNiO_{3-\delta}$ thin films," *J. Phys. Condens. Mat.* **31**(13), p. 135601, 2019.

[40] R. Jaramillo, S. D. Ha, D. Silevitch, and S. Ramanathan, "Origins of bad-metal conductivity and the insulator-metal transition in the rare-earth nickelates," *Nat. Phys.* **10**(4), pp. 304–307, 2014.

[41] J. Bruin, H. Sakai, R. Perry, and A. Mackenzie, "Similarity of scattering rates in metals showing T-linear resistivity," *Science* **339**(6121), pp. 804–807, 2013.

[42] P. Giraldo-Gallo, J. Galvis, Z. Stegen, K. A. Modic, F. Balakirev, J. Betts, X. Lian, C. Moir, S. Riggs, J. Wu, *et al.*, "Scale-invariant magnetoresistance in a cuprate superconductor," *Science* **361**(6401), pp. 479–481, 2018.

[43] A. A. Patel and S. Sachdev, "Theory of a Planckian metal," *Phys. Rev. Lett.* **123**(6), p. 066601, 2019.

[44] J. Zaanen *et al.*, "Planckian dissipation, minimal viscosity and the transport in cuprate strange metals," *SciPost Phys.* **6**(5), p. 061, 2019.

[45] K. Rajeev, G. Shivashankar, and A. Raychaudhuri, "Low-temperature electronic properties of a normal conducting perovskite oxide ($LaNiO_3$)," *Solid State Commun.* **79**(7), pp. 591–595, 1991.

[46] J. Blasco, M. Castro, and J. Garcia, "Structural, electronic, magnetic and calorimetric study of the metal-insulator transition in $NdNiO_{3-\delta}$," *J. Phys. Condens. Mat.* **6**(30), p. 5875, 1994.

[47] E. Mikheev, A. J. Hauser, B. Himmetoglu, N. E. Moreno, A. Janotti, C. G. Van de Walle, and S. Stemmer, "Tuning bad metal and non-Fermi liquid behavior in a Mott material: Rare-earth nickelate thin films," *Sci. Adv.* **1**(10), p. e1500797, 2015.

[48] J. Liu, M. Kargarian, M. Kareev, B. Gray, P. J. Ryan, A. Cruz, N. Tahir, Y.-D. Chuang, J. Guo, J. M. Rondinelli, *et al.*, "Heterointerface engineered electronic and magnetic phases of $NdNiO_3$ thin films," *Nat. Commun.* **4**(1), pp. 1–11, 2013.

[49] H. Kobayashi, S. Ikeda, Y. Yoda, N. Hirao, Y. Ohishi, J. Alonso, M. Martinez-Lope, R. Lengsdorf, D. Khomskii, and M. Abd-Elmeguid, "Pressure-induced unusual metallic state in $EuNiO_3$," *Phys. Rev. B* **91**(19), p. 195148, 2015.

[50] E. Yadav, S. Harisankar, K. Soni, and K. Mavani, "Influence of Cu doping and thickness on non-Fermi liquid behaviour and metallic conductance in epitaxial $PrNiO_3$ thin films," *Appl. Phys. A* **124**(9), p. 614, 2018.

[51] V. E. Phanindra, P. Agarwal, and D. Rana, "Terahertz spectroscopic evidence of non-Fermi-liquid-like behavior in structurally modulated $PrNiO_3$ thin films," *Phys. Rev. Mater.* **2**(1), p. 015001, 2018.

[52] S. Stemmer and S. J. Allen, "Non-Fermi liquids in oxide heterostructures," *Rep. Prog. Phys.* **81**(6), p. 062502, 2018.

[53] G. Herranz, V. Laukhin, F. Sánchez, P. Levy, C. Ferrater, M. García-Cuenca, M. Varela, and J. Fontcuberta, "Effect of disorder on the temperature dependence of the resistivity of $SrRuO_3$," *Phys. Rev. B* **77**(16), p. 165114, 2008.

[54] N. D. Patel, A. Mukherjee, N. Kaushal, A. Moreo, and E. Dagotto, "Non-Fermi liquid behavior and continuously tunable resistivity exponents in the Anderson-Hubbard model at finite temperature," *Phys. Rev. Lett.* **119**(8), p. 086601, 2017.

[55] Q. Guo, S. Farokhipoor, C. Magén, F. Rivadulla, and B. Noheda, "Tunable resistivity exponents in the metallic phase of epitaxial nickelates," *Nat. Commun.* **11**(1), pp. 1–9, 2020.

[56] K. Lee, A. Patel, N. Trivedi, and S. Sachdev, "Emergent interacting two-fluids in a disordered Hubbard model," *APS* **2019**, pp. H06–005, 2019.

[57] K. Lee, A. Patel, N. Trivedi, and S. Sachdev, "Microscopic origin of the 'strange' metal," *Bulletin of the American Physical Society* **65**, 2020.

[58] S. Kumar and P. Majumdar, "Singular effect of disorder on electronic transport in strongly coupled electron-phonon systems," *Phys. Rev. Lett.* **94**(13), p. 136601, 2005.

[59] N. F. Mott, "Conduction in non-crystalline materials: Iii. localized states in a pseudogap and near extremities of conduction and valence bands," *Philos. Mag.* **19**(160), pp. 835–852, 1969.

[60] I. Shlimak, *Is Hopping a Science? Selected Topics of Hopping Conductivity*, World Scientific, 2015.

[61] D. J. Bergman and D. Stroud, "Physical properties of macroscopically inhomogeneous media," in *Solid State Phys.*, **46**, pp. 147–269, Elsevier, 1992.

[62] P.-H. Xiang, N. Zhong, C.-G. Duan, X. Tang, Z. Hu, P. Yang, Z. Zhu, and J. Chu, "Strain controlled metal-insulator transition in epitaxial $NdNiO_3$ thin films," *J. Appl. Phys.* **114**(24), p. 243713, 2013.

[63] G. Catalan, R. Bowman, and J. Gregg, "Metal-insulator transitions in $NdNiO_3$ thin films," *Phys. Rev. B* **62**(12), p. 7892, 2000.

[64] M. L. Medarde, "Structural, magnetic and electronic properties of $RNiO_3$ perovskites (R= rare earth)," *J. Phys. Condens. Mat.* **9**(8), p. 1679, 1997.

[65] P. Laffez, M. Zaghrioui, I. Monot, T. Brousse, and P. Lacorre, "Microstructure and metal-insulator transition of $NdNiO_3$ thin films on various substrates," *Thin Solid Films* **354**(1-2), pp. 50–54, 1999.

[66] X. Granados, J. Fontcuberta, X. Obradors, and J. Torrance, "Metastable metallic state and hysteresis below the metal-insulator transition in $PrNiO_3$," *Phys. Rev. B* **46**(24), p. 15683, 1992.

[67] S. Liu, B. Phillabaum, E. Carlson, K. Dahmen, N. Vidhyadhiraja, M. Qazilbash, and D. Basov, "Random field driven spatial complexity at the Mott transition in VO_2," *Phys. Rev. Lett.* **116**(3), p. 036401, 2016.

[68] A. Legros, S. Benhabib, W. Tabis, F. Laliberté, M. Dion, M. Lizaire, B. Vignolle, D. Vignolles, H. Raffy, Z. Li, *et al.*, "Universal T-linear resistivity and Planckian dissipation in overdoped cuprates," *Nat. Phys.* **15**(2), pp. 142–147, 2019.

[69] Y. Nakajima, T. Metz, C. Eckberg, K. Kirshenbaum, A. Hughes, R. Wang, L. Wang, S. R. Saha, I.-L. Liu, N. P. Butch, *et al.*, "Quantum-critical scale invariance in a transition metal alloy," *Commun. Phys.* **3**(1), pp. 1–8, 2020.

[70] O. Gunnarsson, M. Calandra, and J. Han, "Colloquium: Saturation of electrical resistivity," *Rev. Mod. Phys.* **75**(4), p. 1085, 2003.

[71] S. D. Ha, R. Jaramillo, D. Silevitch, F. Schoofs, K. Kerman, J. D. Baniecki, and S. Ramanathan, "Hall effect measurements on epitaxial $SmNiO_3$ thin films and implications for antiferromagnetism," *Phys. Rev. B* **87**(12), p. 125150, 2013.

[72] Y. Cao, D. Chowdhury, D. Rodan-Legrain, O. Rubies-Bigorda, K. Watanabe, T. Taniguchi, T. Senthil, and P. Jarillo-Herrero, "Strange metal in magic-angle graphene with near Planckian dissipation," *Phys. Rev. Lett.* **124**(7), p. 076801, 2020.

[73] M. Hooda and C. Yadav, "Electronic properties and the nature of metal-insulator transition in $NdNiO_3$ prepared at ambient oxygen pressure," *Physica B: Condensed Matter* **491**, pp. 31–36, 2016.